Outlier Detection for 3D-Mapping-Aided GNSS Positioning

Qiming Zhong, Paul Groves
University College London, United Kingdom

BIOGRAPHY

Qiming Zhong is a PhD student at University College London (UCL), specializing in 3D-mapping-aided GNSS. He holds a BSc in Electrical and Electronic Engineering from the University of Nottingham, Ningbo, China and an MSc in Robotics and Computing from UCL. (q.zhong.17@ucl.ac.uk)

Dr Paul Groves is an Associate Professor at UCL, where he leads a program of research into robust positioning and navigation. He is interested in all aspects of navigation and positioning, including multi-sensor integrated navigation, improving GNSS performance under challenging reception conditions, and novel positioning techniques. He is author of the book Principles of GNSS, Inertial and Multi-Sensor Integrated Navigation Systems. He is the recipient of the 2016 Institute of Navigation Thurlow Award and a Fellow of the Royal Institute of Navigation. He holds a bachelor's degree and doctorate in physics from the University of Oxford. (p.groves@ucl.ac.uk)

ABSTRACT

This paper takes 3D-mapping-aided (3DMA) GNSS as an example and investigates the outlier detection for pattern matching based positioning. Three different test statistics, two in the measurement domain and one in the position domain, are presented. Two 3D city maps with different levels of detail were used, one of which contained two obvious errors, to demonstrate the performance of 3DMA GNSS positioning in the presence of errors in the mapping data. The experiments tested were conducted alongside busy roads in the London Borough of Camden, where a total of 8 sets of 2-minute static pedestrian navigation data were collected with a u-blox EVK M8T GNSS receiver. The results confirm that both 3D mapping errors and temporary environmental changes (such as passing vehicles) can have a significant negative impact on the performance of 3DMA GNSS positioning. After applying outlier detection, single-epoch 3DMA GNSS algorithm reduces the horizontal RMS position error by approximately 15% compared to that without outlier detection. The filtering algorithm attenuates the effects of temporary environmental changes, providing an improvement of about 15% over single-epoch positioning, while the outlier algorithm further reduces the RMS error to a comparable level to that of using high-accuracy maps, about 4.7m.

I. INTRODUCTION

Pattern matching is one of the techniques commonly used in the field of navigation and positioning. Applications based on pattern matching, such as Wi-Fi positioning, image matching and terrain-referenced navigation [1], are well known as typical examples. These techniques start by delineating a range of candidate positions and then compare predictions made by mapping or other databases with actual observations to score these candidates and give a positioning solution.

Pattern matching techniques are also being applied to GNSS positioning in challenging environments. In urban canyons, the performance of conventional GNSS navigation and positioning is unsatisfactory for a range of applications such as pedestrian and vehicle navigation, with horizontal position errors in some extreme cases exceeding tens of metres [2, 3]. Non-line-of-sight (NLOS) reception and multi-path effects are often considered to be two important culprits in the corruption of GNSS performance [1–5]. Some studies have demonstrated different 3D-mapping-aided (3DMA) GNSS techniques that can significantly improve GNSS positioning accuracy in urban environments [4, 6–9]. Many of these techniques score candidate positions by comparing observations with predictions of satellite visibility and/or signal propagation path made from 3D building models, which are typical applications of pattern matching-based positioning.

The quality of the prediction strongly influences the performance of pattern matching. However, the reliability and resilience of the mapping data itself is often overlooked. The mapping data may be incorrect for various reasons. One of the intuitive points is that the environment may be changing all the time, but the mapping data cannot be updated in a timely manner. Temporary changes in the environment, such as road construction, temporarily parked cars, etc., are not usually included in the mapping database. This paper therefore investigates outlier detection for positioning techniques based on pattern matching, focusing on 3DMA GNSS.

An outlier refers to a measurement that shows a large error due to a fault somewhere. In 3DMA GNSS, predictions inevitably

contain some errors because it is impossible for mapping to provide a complete and accurate representation of the surrounding environment. Incorrect predictions may arise from errors in the 3D mapping data itself. The level of detail (LoD) and accuracy of geographical data depends to a large extent on the nature of the data, spatial scale, acquisition technique, and available funding [10]. The lagging nature of the mapping data may result in new buildings and temporary structures being omitted and recently demolished buildings being included. In addition, some random environmental variations that are not included in the mapping data but have an impact on the GNSS signal, such as passing vehicles and street furniture, can also lead to incorrect predictions. Current 3DMA GNSS algorithms usually just treat them as noise sources. One or two erroneous predictions in an epoch usually have a limited impact on the position solution. Excessive prediction errors, however, normally degrade the positioning accuracy. Outlier detection is therefore needed to identify and exclude potentially affected measurements.

There are many applications that could benefit from this work. Those applications where 3DMA GNSS positioning can be applied could gain performance improvements, such as navigation for pedestrians and vehicles, emergency call location for people and vehicles, navigation for the visually impaired, location-based services, mobile gaming, etc. Other applications based on pattern matching, such as indoor positioning based on signal characteristics, can also draw some ideas or inspiration from this work.

This paper has been divided into 5 sections. In Section II, various 3D mapping-based GNSS positioning methods are briefly reviewed, followed by a discussion of the necessity of outlier detection for 3DMA GNSS and some common approaches to detecting outliers. Then, in Section III, two outlier detection methods designed based on the characteristics of 3DMA GNSS are proposed. Section IV presents the test results of a GNSS dataset collected from multiple test sites in London. The position solutions using different outlier detection methods are compared. In addition, the results without any outlier detection are included as a reference. Finally, the conclusions are summarised in Section V.

II. BACKGROUND

In an open environment, stand-alone GNSS can provide location solutions with an accuracy of within a few metres. In urban canyons, however, the complex environment makes it almost impossible for GNSS to deliver its full capability. Tall buildings and leafy trees on each side of the road, together with large vehicles travelling on the road, all affect the satellite signal propagation to varying degrees. In particular, the negative effects of blocking and reflections caused by buildings are significant [3, 11, 12]. The phenomenon of receiving a mixture of line-of-sight (LOS) and reflected signals is known as multipath interference, while the phenomenon of receiving only reflected signals is known as non-line-of-sight (NLOS) reception [1]. The frequent occurrence of these two phenomena are two key reasons for the frustration of conventional GNSS positioning in cities [1–5].

II.1. 3D-Mapping-Aided GNSS

A building can be represented at different levels of detail (LoD), as shown in Figure 1. It can be depicted as a 3D prismatic solid with a unique height (LoD1), but can also be abstracted as a footprint or roof print (LoD0), or as a more detailed 3D mesh with a standard type, generalized roof (LoD2), or even as an delicate architectural model without restrictions (LoD3) [13, 14]. The additional information that 3D building data brings to positioning and navigation includes, but is not limited to, building location, building orientation and roof height, enriches and enables new methods for dealing with issues such as multipath and NLOS reception that often occur in urban environments.

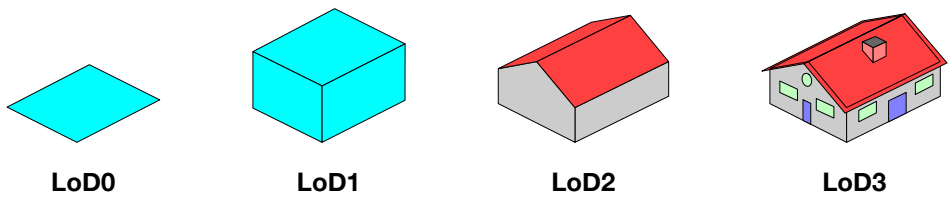

Figure 1: Representation of the same building at different LoDs (CityGML 3.0)

Over the past decade, there has been a lot of interest in 3DMA GNSS. This improves performance in dense urban areas by using maps of the buildings to predict which signals are directly visible at any given location. Many different approaches have been demonstrated. According to the different principles of solution determination, they can be divided into shadow matching and 3DMA ranging. The former uses the signal strength measurements, while the latter uses the pseudo-ranges similar to the conventional GNSS method.

Shadow matching adopts the idea of pattern matching and determines the solution by comparing the received signal strength with the satellite visibility prediction at a series of candidate positions. The concept was independently proposed by four different research groups [15–18], and the authors of [19, 20] then initially demonstrated the potential of shadow matching technique in

cross-street positioning with an accuracy of several metres. All of the different research groups that have worked on shadow matching have converged on the approach of hypothesis testing. The main difference lies in the methods of scoring candidate positions and obtaining the overall position solution from the candidate position scores. In the early research [21], the measured satellite visibility is a binary value obtained by a hard threshold on the SNR value. The degree of matching between the visibility prediction and measurement used the exclusive not or (XNOR) logical operation that returns true if its inputs are the same, otherwise false. The position solution is determined by a weighted average of the coordinates of several candidate points with high scores. Some subsequent studies [20,22–24] have shown better performance using probability-based satellite visibility and Bayesian theory-based matching determination. Some different research groups have also demonstrated continuous positioning based on particle filtering [23,25].

There are many different approaches to 3DMA ranging. Among them, one of the most intuitive approaches is to exclude the NLOS signals detected by using 3D models from the calculation [26–28]. These methods require a fairly accurate initial position to enable subsequent NLOS detection algorithms to confidently predict satellite visibility without much time. In urban environments, most positioning applications cannot provide a sufficiently accurate solution within a few seconds after launching. Therefore, these methods are mostly used in continuous positioning.

Many research groups tend to use NLOS measurements instead of simply deleting them. Hypothesis testing is one of the commonly used methods. At a series of candidate positions generated around a rough position solution, the path delay of the NLOS signal can be estimated by the 3D building model. These candidate positions are then scored based on the path prediction and the actual measurement [7, 29–31]. However, the primary limitation of these approaches is that the propagation path calculation requires a large amount of computing resources. The pseudo-range error distribution of the LOS signal conforms to a symmetric distribution, while the counterpart of the NLOS signal is asymmetric. A version of likelihood-based ranging is proposed [6] to use a different combination of error distributions at each candidate position based on the visibility predictions from 3D mapping data, which enables those NLOS pseudo-ranges to participate in the position calculation without explicitly computing the additional distance travelled by them.

II.2. UCL's 3DMA GNSS Core Algorithms

UCL's 3DMA GNSS algorithms consist mainly of shadow matching (SM), likelihood-based ranging (LBR) and an integration algorithm, as shown in Figure 2. Both SM and LBR are performed in the way of hypothesis testing on the candidate positions. The candidate positions are a set of three-dimensional coordinates. For land positioning and navigation applications, in order to reduce the complexity of the problem, the height dimension is set to the sum of the terrain height at that horizontal position and the height of the user device above the ground.

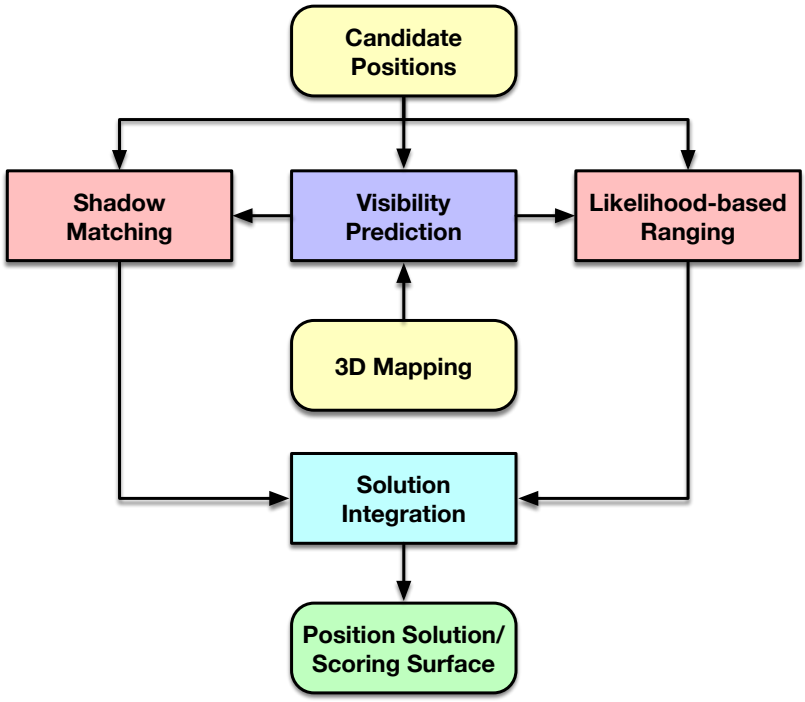

Figure 2: Components of the 3DMA GNSS Core Algorithms

3D mapping data is used to predict the visibility of each satellite signal (i.e., LOS or NLOS) at each candidate position. This step is relatively computationally intensive and time consuming. Therefore, an intermediate product called building boundaries has been introduced to achieve the goal of being able to operate in real time over a large number of candidate positions. The building boundary (BB) refers to the maximum elevation of all buildings within a certain distance at a given azimuth. In other words, it is the minimum elevation of a satellite that allows users to receive its signals directly in that direction. The building boundary is pre-computed and stored for each candidate position. When required, the signal can be classified as LOS or NLOS by simply comparing the satellite elevation with the building boundary at the corresponding azimuth.

The shadow matching (SM) algorithm [20] compares the satellite visibility predictions with the counterpart determined by the received signal strength to calculate the degree of matching at different candidate positions, thereby giving the optimal solution. The algorithm comprises the following steps [6, 20]:

- The predicted visibility of each satellite signal at each candidate position is obtained.
- For each received signal, the probability that it is direct LOS is determined from the measurement of C/N_0 using an appropriate statistical model.
- A matching score is obtained by evaluating each satellite at each candidate position based on the match between its predicted visibility to measured C/N_0.
- The final score for each candidate position is a combination of the matching scores for each satellite at that position.

The likelihood-based ranging (LBR) algorithm [6] applies different statistical distributions to pseudo-range errors according to satellite visibility predictions, and then evaluates the correspondence between the measured and predicted pseudo-ranges to give the positioning solution. The algorithm comprises the following steps [6]:

- The predicted visibility of each satellite signal at each candidate position is obtained.
- At each candidate position, one of the satellites predicted to be direct LOS is selected as the reference.
- At each candidate position, the measurement innovation for each satellite is obtained by subtracting the direct LOS range and some known errors, such as satellite clock errors, atmospheric delays and inter-constellation offsets, from the measured pseudo-range, and then differencing with respect to the reference satellite to remove receiver clock offset.
- At each candidate position, the cumulative probability of the measurement innovation on a skew-normal distribution is determined for each satellite predicted to be NLOS. These NLOS innovations are then replaced by corresponding direct LOS innovations with the same cumulative probability.
- The final score for each candidate position is calculated using the modified measurement innovations and their error covariance matrix.

As shown in Figure 3, the intention of SM is to improve the accuracy in the direction perpendicular to the street, whereas LBR is considered to be more accurate in the direction along the street. Therefore, a hypothesis-domain integration algorithm is executed to give a comprehensive single score for each candidate position based on the scoring surfaces from SM and LBR. Finally, the position solution is obtained by using the combined scores to weight the candidate positions.

Filtered solutions are used in almost all pedestrian and vehicle navigation applications. Compared to single epoch positioning, the filtering algorithm delineates a better search area and provides a priori for the current solution based on the position and velocity solution from the previous epoch. Therefore, the filtered solution is more accurate and reliable compared to the single-epoch one.

Two multi-epoch 3DMA GNSS algorithms have been described in detail in [32]. Since 3DMA GNSS particle filtering and grid filtering have similar performance, only the results of particle filtering are demonstrated in this paper. Figure 4 shows the six stages of the 3DMA GNSS particle filter with outlier detection applied.

In contrast to the particle filtering algorithm described in [32], the algorithm used in this paper introduces one of the outlier detection techniques mentioned in sections III.2 and III.3 during the initialisation and 3DMA GNSS scoring stages, while all other parts remain the same.

The initialisation of the 3DMA GNSS particle filter is made up of two components: position and velocity. The position initialisation uses a single-epoch 3DMA GNSS positioning algorithm with outlier detection, followed by sampling the likelihood surface to generate a set of particles with equal weights. The velocity is initialised by least-squares estimation from pseudo-range rate measurements weighted by the corresponding signal strength and average LOS probability. During the system propagation step, the state estimate of each particle changes according to a predetermined system transition model, while its probability remains constant. Particles can be treated as candidate positions in the 3DMA GNSS algorithm. Subsequently, the 3DMA scores for each particle can be determined by shadow matching, likelihood-based ranging and hypothesis-domain integration,

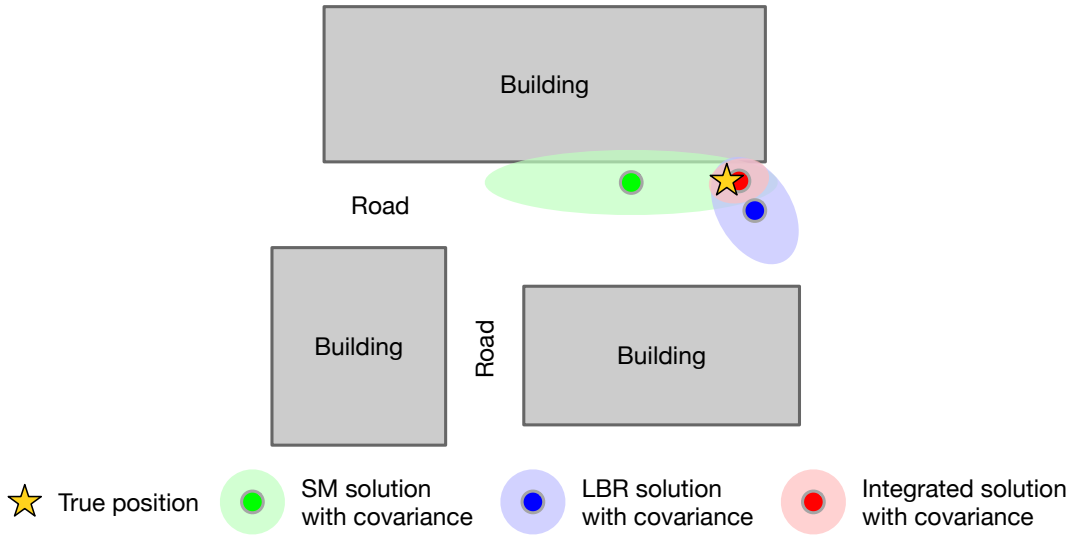

Figure 3: Schematic diagram of 3DMA GNSS positioning

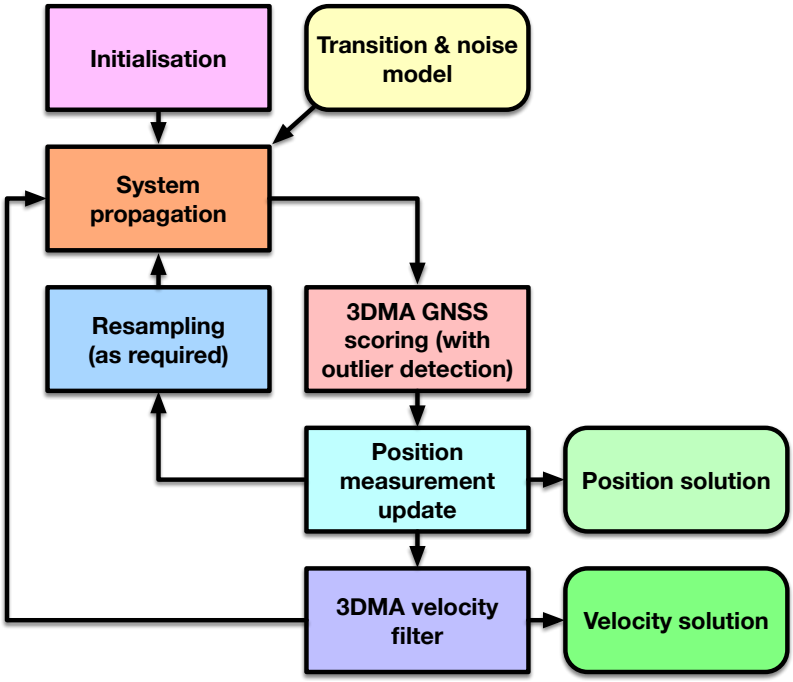

Figure 4: Components of particle filter-based 3DMA GNSS algorithm with outlier detection

supplemented by 3DMA outlier detection. In the position measurement update stage, the weight for each particle is updated with the propagated likelihood and the newly calculated 3DMA scores, and the filtered position solution is obtained by the weighted average position of the particles. The velocity and clock drift are maintained by an extended Kalman filter, where the velocity state estimate is held constant with increasing error covariance in the prediction step and the measurement error is weighted according to the measured signal strength and average LOS probability in the update step. Finally, particles are re-sampled as required according to the likelihood distribution to remove the low weights and duplicate the high weights to attenuate the degeneration problem.

A more detailed description of the above algorithms can be found in [6, 32]. Single-epoch 3DMA GNSS has been demonstrated in Canary Wharf [6], and a multi-epoch version incorporating either particle or grid filtering has been demonstrated in the City of London and Canary Wharf [32].

II.3. The Need for Outlier Detection

An outlier is an observation that appears to deviate significantly from the other members of the sample in which it is located [33, 34]. In navigation, outliers may cause corruption of the position solution. A robust navigation system therefore usually contains modules to detect and eliminate (or correct if possible) outlying measurements [1].

There are many reasons for outliers. An outlier sometimes indicates erroneous data. For example, GNSS observations may not have been collected correctly due to human and instrument error. An outlier may also arise from factors that have been neglected. In an urban environment, the blocking and reflecting effects on satellite signals are important causes of outliers. In 3DMA GNSS, 3D city models are therefore used to predict satellite visibility and, in some studies, to estimate reflection paths. With this aiding information, many outlier measurements can be justifiably removed or even corrected. However, this auxiliary information is not perfect. Errors will inevitably occur in the generation of these aiding data, potentially resulting in new outliers. Incorrect 3D aids may limit improvements in positioning performance and in some cases even have a negative impact. Consequently, outlier detection for 3D aiding information is necessary to help improve the reliability of 3DMA techniques, which eventually benefits positioning accuracy.

Some outliers arise because of the 3D city model used. 3DMA techniques rely heavily on the LoD and accuracy of the models used. Inaccurate mapping data may directly produce incorrect aiding information. First, the LoD of the model deserves to be noted. Figure 5 illustrates the blocking effect of a building model with different LoDs on the signal from a given satellite. Receivers in the shadow will be assumed not to receive the LOS signal from that satellite. The shadow outlined in green is from the LoD2 model, while the one outlined in red is from the LoD1 model. It can be clearly seen that the models with different LoDs leave different shadows, with the non-overlapping parts being filled in with red and green. As a result, 3DMA GNSS can produce incorrect aiding information over the red shaded areas.

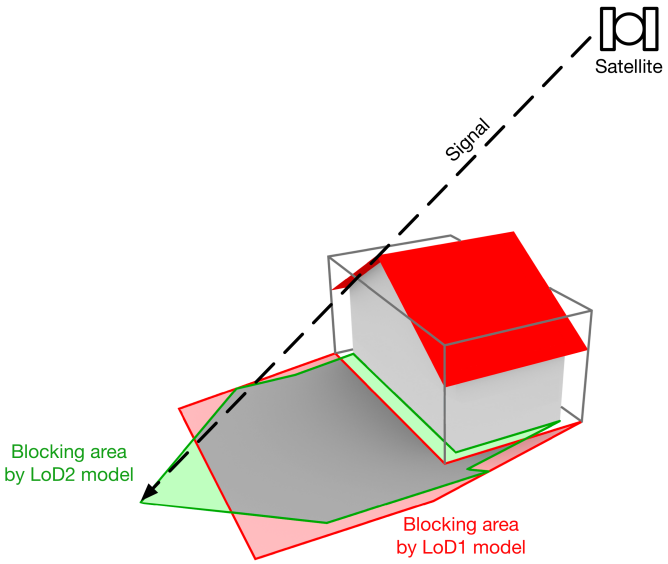

Figure 5: Signal blocking areas for the LoD1 and LoD2 models (outlined in red and green, respectively) of a building
*The figure is adapted from [35]

Second, there may be some measurement errors in the building model, including but not limited to building coordinates, orientation and height attributes. Building height data, for instance, can be easily converted into LoD1 building models. Ordnance Survey (OS) and OpenStreetMap (OSM) are two popular providers of building height information in the UK. OS directly provides building heights with an error of 2.4 m at 99% confidence level [36], while OSM provides height information for only some of the buildings, with the remaining building heights being deduced from the number of above-ground levels.

Finally, the 3D models may suffer from being out of date. Any 3D model has a certain update interval, for example, the building height attributes provided by Ordnance Survey are updated every six months [37]. In the interval between updates, any newly constructed buildings will be omitted from the database, and newly demolished ones will be retained. The height of buildings under construction may change significantly on a weekly or even daily basis, further challenging the timeliness of updates to the 3D model.

Outliers may also be caused by some unmapped obstacles. These obstacles are not usually included in the 3D model, but can indeed lead to inaccurate 3D aiding information. For instance, the satellite signal may be temporarily blocked by large vehicles

passing in an adjacent lane, or by large, leafy trees on the roadside. These unmapped objects may cause inaccurate predictions of satellite visibility and signal propagation path based on the 3D model alone, affecting the accuracy of positioning.

II.4. Outlier Detection Methods

In conventional GNSS positioning, consistency checking is one of the most common outlier detection techniques and has been integrated by many modern receivers into their fault detection and exclusion (FDE) modules. This technique is based on the assumption that measurements from direct LOS signals exhibit better consistency in the positioning solution than those from NLOS and severely multipath contaminated signals [1]. In single-epoch GNSS positioning, consistency is usually quantified in the measurement domain by the normalized residual:

$$\delta z'^j = \frac{\left|\delta z^j\right|}{\sigma^j} \tag{1}$$

where δz^j is the residual of the measurement from satellite j, and σ^j is the associated standard deviation. The residual refers to the difference between the measurement, $\tilde{\rho}$, and the prediction of its measurement obtained from the least squares solution, $\hat{\rho}$, given by

$$\delta z^j = \tilde{\rho}^j - \hat{\rho}^j \tag{2}$$

The corresponding standard deviation is usually an empirically determined constant or a value based on signal strength and/or satellite elevation. In general, a smaller ratio from Equation (1) indicates better consistency and a lower fault probability for the corresponding measurement. Thus, the ratios from all observations are compared with a predefined threshold and those exceeding the threshold are labelled and rejected as outliers.

However, the residuals are sensitive to outliers. An outlying measurement may lead to large residuals for some other non-faulty measurements, resulting in good measurements being incorrectly excluded. A commonly used method to mitigate this issue is sequential testing. It is an iterative process where in each iteration the measurement with the largest residual is rejected, followed by recalculating new residuals with the remaining measurements until all residuals fall within the threshold or there are not enough measurements for outlier detection.

Sequential testing based on individual residuals can also sometimes incorrectly reject good observations, since the largest residual does not always correspond to a bad measurement, especially in the presence of multiple outliers. An enhanced version of the sequential testing is to perform a chi-square test on the measurement residuals as a whole. The vector consisting of residuals is assumed to be an m-dimensional Gaussian random vector with a mean of 0 and a covariance of $\mathbf{C}_{\delta\mathbf{z}}$, and hence the square of its Mahalanobis distance to the origin is chi-squared distributed with m degrees of freedom. The test statistic is therefore given by

$$s^2 = \delta\mathbf{z}^{\mathrm{T}}\mathbf{C}_{\delta\mathbf{z}}^{-1}\delta\mathbf{z} \tag{3}$$

where $\delta\mathbf{z}$ is the residual vector, and $\mathbf{C}_{\delta\mathbf{z}}$ is the covariance matrix. When the test statistic exceeds a threshold, each of the parallel solutions that exclude an observation is calculated, and the one with the lowest chi-square test statistic is accepted. The process is iterated until the test statistic falls below the threshold.

An alternative to the "top-down" sequential testing approach is the "bottom-up" subset comparison [38]. The "bottom-up" method starts by taking a subset of measurements and then expands the subset by adding additional measurements that are consistent with it. The quality of the subset is important for this type of method, as a minimal subset adulterated with faulty observations may directly degrade the performance of outlier detection.

In addition to the measurement domain, outlier detection can also be performed in the position domain. Combinations of measurements containing outliers usually give different position solutions than those without fault observations. Therefore, solutions can be calculated separately using different combinations of measurements and compared with each other. If two solutions are significantly different, it is reasonable to assume that the measurement used to calculate one solution but not the other may be an outlier.

3DMA GNSS works in a different way to conventional GNSS positioning techniques. Essentially, 3DMA GNSS evaluates the similarity between the observations, including pseudo-range and signal strength, and the predictions made from the 3D mapping data on an array of candidate positions, and derives a solution based on the distribution of similarity. As conventional residuals are not present in 3DMA GNSS, the residual-based outlier detection commonly used in conventional GNSS positioning is not applicable at all. Therefore, 3DMA GNSS requires some new methods of outlier detection based on its own characteristics.

III. PROPOSED OUTLIER DETECTION METHODS

Several different test statistics in the measurement and position domains are proposed for shadow matching (SM) and likelihood-based ranging (LBR). Then sequential testing and subset comparison methods are presented in Sections III.2 and III.3, respectively.

III.1. Test Statistic

UCL's 3DMA GNSS positioning algorithm contains two positioning modules, shadow matching (SM) and likelihood-based ranging (LBR), which employ two different types of measurements, C/N_0 and pseudo-range, respectively, to calculate the position solution. Therefore, different test statistics need to be designed for each of them in their respective measurement domains.

The main idea of the test statistic in the measurement domain is to use the 3DMA GNSS solution obtained from a subset of measurements to estimate the excluded measurements, and the outlying measurements should be significantly different from their corresponding predictions.

The test statistic for SM, ${S^j_{SM}}^2$, in the measurement domain is then derived by comparing the LOS probability estimated from the C/N_0 measurement with that given by the building boundary averaged over the position solution distribution calculated with the other measurements,

$${S^j_{SM}}^2 = \frac{\left[p(LOS|C/N_0)^j - \bar{p}(LOS|BB)^j\right]^2}{\sigma_v^2} \tag{4}$$

where σ_v is the standard deviation of the difference in satellite visibility, $p(LOS|C/N_0)^j$ is the inferred LOS probability of satellite j based on its C/N_0 measurement (please see Appendix A.3 in [6] for details), $\bar{p}(LOS|BB)^j$ is the average LOS probability based on the building boundary data at the azimuth and elevation where satellite j is located, and σ_v is the standard deviation of the difference in satellite visibility, given by,

$$\bar{p}(LOS|BB)^j = \frac{\sum_p \Lambda_p^{-j} p(LOS|BB)^j_p}{\sum_p \Lambda_p^{-j}} \tag{5}$$

$$\sigma_v = \frac{p(LOS|BB)_{max} - p(LOS|BB)_{min}}{3\sqrt{2}} = \frac{0.9 - 0.1}{3\sqrt{2}} \approx 0.19 \tag{6}$$

where Λ_p^{-j} is the likelihood of candidate position p from the integrated 3DMA GNSS solution calculated with a subset of measurements excluding satellite j, $p(LOS|BB)^j_p$ is the LOS probability from building boundaries at the azimuth and elevation of satellite j, and $p(LOS|BB)_{max} = 0.9$ and $p(LOS|BB)_{min} = 0.1$ are the upper and lower bounds on the LOS probability of the satellite, respectively.

The test statistic for LBR in its measurement domain is determined by the remapped measurement innovation weighted by the same 3DMA GNSS solution as in the SM,

$${S^j_{LBR}}^2 = \frac{{\delta\bar{z}'_j}^2}{\sigma^2_{\delta z,j}} \tag{7}$$

where $\delta\bar{z}'_j$ and $\sigma^2_{\delta z,j}$ are the weighted pseudo-range measurement innovation and its corresponding variance, respectively, given by

$$\delta\bar{z}'_j = \frac{\sum_p \Lambda_p^{-j} \delta z'_{p,j}}{\sum_p \Lambda_p^{-j}} \tag{8}$$

$$\sigma^2_{\delta z,j} = \frac{\sum_p \Lambda_p^{-j} C_{\delta z,p,j}}{\sum_p \Lambda_p^{-j}} \tag{9}$$

where $\delta z'_{p,j}$ is the remapped measurement innovation for satellite j at candidate position p, and $C_{\delta z,p,j}$ is the corresponding measurement error covariance, both of which are obtained from the intermediate step of the LBR (please see Appendix A.4 in [6] for details).

In the position domain, the horizontal radial distance between the SM and LBR solutions is not suitable as the test statistic. This is because, as shown in Figure 3, SM sometimes only contributes to accuracy in the cross-street direction and is susceptible to ambiguity problems at locations with similar sky maps (especially when the number of satellites is small), whereas LBR contributes more to accuracy in the along-street direction.

In cases where SM and LBR perform well, the sky plots above their position solutions are usually very similar. Therefore, the 3DMA position solution can be used to create a vector consisting of the average LOS probabilities, as follows,

$$\bar{\mathbf{p}}(LOS|BB) = \begin{bmatrix} \bar{p}(LOS|BB)^1 & \bar{p}(LOS|BB)^2 & \cdots & \bar{p}(LOS|BB)^j \end{bmatrix}^{\mathrm{T}} \tag{10}$$

where $\bar{p}(LOS|BB)^j$ can be calculated using Equation (5). Note that the size of this LOS probability vector always remains the same as the total number of observed satellites and does not vary with the exclusion of outliers.

After converting into visibility vectors, comparisons between positional solutions will be conducted by comparing the corresponding visibility vectors. Euclidean distance and cosine distance adopt different perspectives (distance and angle respectively) to measure the difference between vectors. Euclidean distances place more emphasis on absolute differences in numerical values, while cosine distances focus more on relative deviations in the direction of the vectors.

The Euclidean distance between vectors **A** and **B** is calculated by,

$$D_E(A,B) = \|\mathbf{A} - \mathbf{B}\| = \sqrt{\sum_i (A_i - B_i)^2} \tag{11}$$

where $\|\cdot\|$ denotes L^2 norm that calculates the distance of the vector coordinate from the origin of the vector space.

The cosine distance between two vectors is computed by,

$$D_C(A,B) = 1 - \frac{\mathbf{A}\cdot\mathbf{B}}{\|\mathbf{A}\|\|\mathbf{B}\|} = 1 - \frac{\sum_i A_i B_i}{\sqrt{\sum_i A_i^2}\sqrt{\sum_i B_i^2}} \tag{12}$$

However, there may be some problems with using cosine distances directly to compare visibility vectors. For example, when $\mathbf{A} = [0.9, 0.9, 0.9]$ and $\mathbf{B} = [0.1, 0.1, 0.1]$, the cosine distance is 0, which is clearly wrong. Therefore, before using Equation (12), the visibility vector need to be pre-processed by joining the original vector, $\bar{\mathbf{p}}(LOS|BB)$, and its complement, $1-\bar{\mathbf{p}}(LOS|BB)$, as follows,

$$\bar{\mathbf{p}}'(LOS|BB) = \begin{bmatrix} \bar{\mathbf{p}}(LOS|BB) \\ 1 - \bar{\mathbf{p}}(LOS|BB) \end{bmatrix} \tag{13}$$

where $\bar{\mathbf{p}}'(LOS|BB)$ is still a vector.

Consequently, the test statistic for 3DMA GNSS positioning in the position domain can be derived by,

$$D = D(LBR, SM) \tag{14}$$

where $D(LBR, SM)$ stands for Euclidean or cosine distance between the visibility vectors consisting of the average satellite visibility calculated from the likelihoods of LBR and SM using Equation (10).

III.2. Sequential Testing Method

The sequential testing method is one of the most commonly used outlier detection methods. It iterates through all the available measurements. At each iteration, a 3DMA position solution is calculated using all available measurements except one that is assumed to be an outlier. The excluded measurement is then evaluated for consistency with the remaining ones in the measurement domain by using Equations (4) and (7). After traversing all measurements, if any inconsistency alarm is raised, the one most inconsistent with the other measurements is excluded. The process is repeated until all measurements pass the consistency check, or there are insufficient measurements left.

The consistency of the measurements is assessed by the SM and LBR in two different dimensions, signal strength and ranging, respectively. Therefore, an integrated test statistic for satellite j to combine the test statistics on the different dimensions is calculated by,

$${S^j_{INT}}^2 = \mathbf{S}^j_X \Sigma_X {\mathbf{S}^j_X}^{\mathrm{T}} \tag{15}$$

where the test statistic vector, $\mathbf{S}^j_X$, is formed by,

$$\mathbf{S}^j_X = \begin{bmatrix} S^j_{SM} & S^j_{LBR} \end{bmatrix} \tag{16}$$

and the weighting matrix, Σ_X, can be the inverse of the covariance matrix calculated by,

$$\Sigma_X = \begin{bmatrix} \sigma_{SM}^2 & 0 \\ 0 & \sigma_{LBR}^2 \end{bmatrix}^{-1} \tag{17}$$

$$\sigma_{SM}^2 = \frac{1}{N_{in}-1} \sum_{j}^{N_{in}} {S_{SM}^j}^2 \tag{18}$$

$$\sigma_{LBR}^2 = \frac{1}{N_{in}-1} \sum_{j}^{N_{in}} {S_{LBR}^j}^2 \tag{19}$$

where N_{in} is the number of satellites to be examined, and the test statistics for both SM and LBR are assumed to be normally distributed with zero mean. The largest integrated test statistic is then compared to an empirically determined threshold to determine whether to exclude the corresponding satellite. The determination of this threshold is discussed in Section IV.2.

III.3. Subset Comparison Method

The subset comparison method is introduced as an alternative to the sequential method for consistency checking. Figure 6 illustrates the flowchart for 3DMA GNSS outlier detection based on the random sample consensus (RANSAC) algorithm.

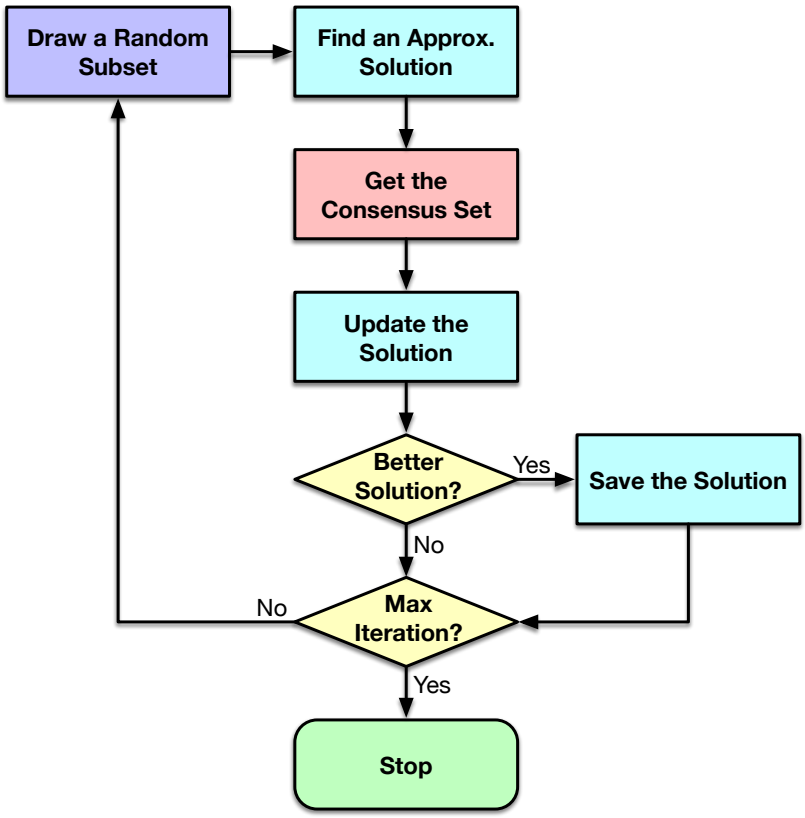

Figure 6: Components of the RANSAC-based outlier detection algorithm

First, a subset is randomly drawn from all the measurements, from which a 3DMA position solution is calculated. Among the remaining measurements, Equations (4) and (7) are used to quantify their consistency with the subset solution, with the 3DMA GNSS solutions used in Equations (5), (8) and (9) being calculated using the subset only. A threshold is then introduced, below which measurements are determined to be consistent with the subset solution and are admitted to the subset to constitute a consensus set (CS). The choice of this threshold is described in Section IV.2. The position solution is subsequently updated based on the newly generated CS and its quality is evaluated by a loss function (also known as a cost function). The cost, C_R,

is derived from the test statistic, D, in the position domain (i.e., Equation (14)) and is given by

$$C_R = D \Big/ \alpha^{N_{CS}} \tag{20}$$

where N_{CS} is the number of elements in the consensus set, and α is the weighting factor, usually taking a value greater than or equal to 1. The value of α is set to 1 in the following experiment, indicating that the cost is independent of the number of elements. Finally, the whole process is repeated until a solution with a sufficiently low cost is found, or the number of iterations reaches the upper limit. The solution with the lowest cost is determined as the final solution.

IV. EXPERIMENTAL TESTS

IV.1. Experimental Setup

A number of experiments were conducted in Camden, London to demonstrate the proposed outlier detection algorithms. The 3D building models used for testing included the LoD1 model provided by Ordnance Survey (OS) and the LoD2 model provided by BlueSky (BS). In the test environment shown in Figure 7, the University College Hospital (UCH) building and the UCL Cruciform Building are highlighted because of their significantly different representations on the OS and BS maps.

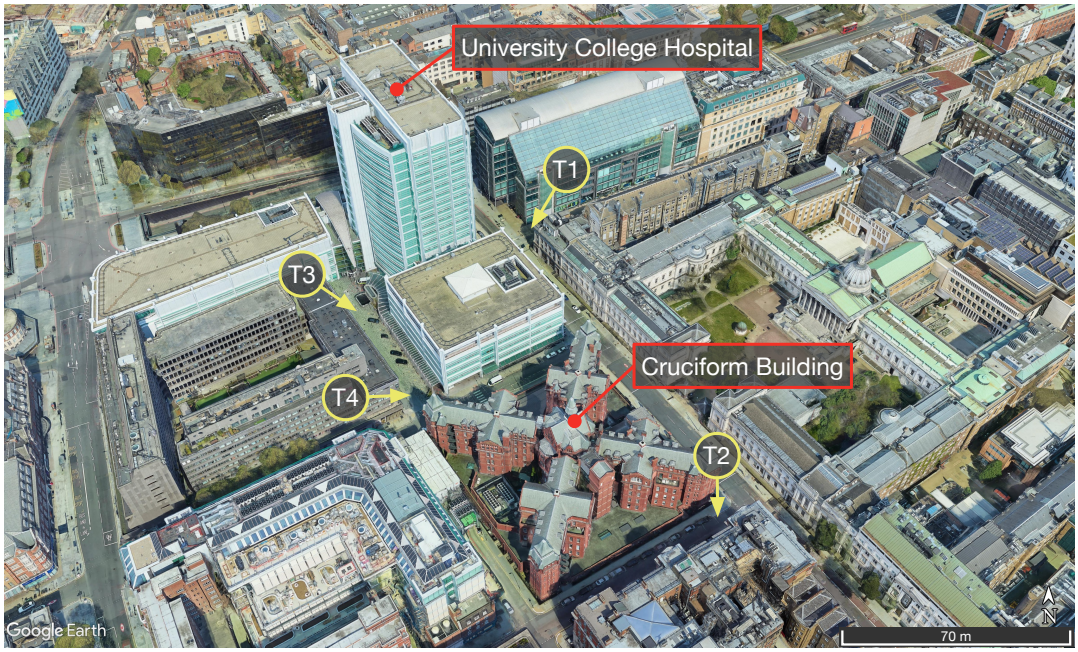

Figure 7: Test environment (background image captured from ©Google Earth)

Figure 8 shows the relative heights of the buildings in the test environment. The dark blue blocks in the figure represent the ground, whose absolute height is set to 0 (as a reference), while the other blocks represent the buildings, whose colour indicates their relative height to the ground.

The UCH building is approximately 80 metres tall and is significantly taller than the two buildings adjacent to it, which is consistent with the height shown on the BS map. However, the height of the UCH building is only about 25 metres in the OS map, which is completely inconsistent with the reality. The Cruciform Building, slightly below the UCH building, is cross-shaped according to the aerial photograph in Figure 7. The shape of the building is more correctly modelled on the BS map than on the OS map where it is simply abstracted as a square.

Several experimental sites around the mismapped buildings were selected, with yellow arrows in Figure 7 marking their locations. On each side of the street at each test site, a u-blox EVK M8T GNSS receiver was used to collect 2 minutes of GNSS data from the three constellations of GPS, GLONASS and Galileo at a recording frequency of 1 Hz. The antenna was placed stationary at 1.1 metres above the ground. The relative distances from the antenna to nearby landmarks were measured by a laser rangefinder, and the coordinates of the true positions were subsequently extracted from the Ordnance Survey MasterMap in the form of east and north on the OSGB36 datum.

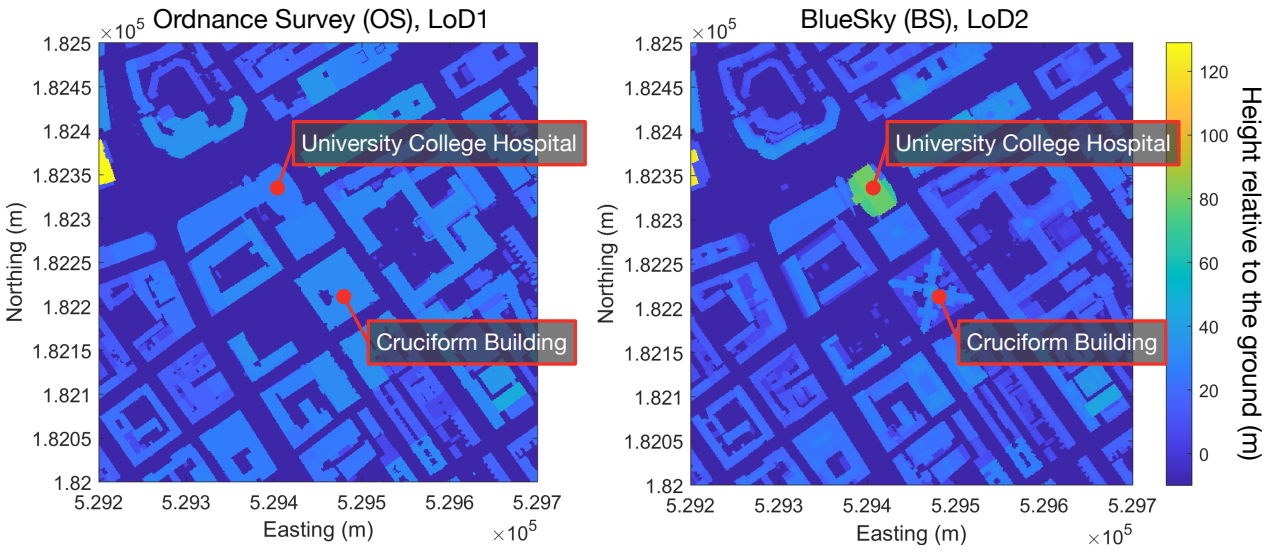

Figure 8: Height maps generated from the Ordnance Survey (OS) and BlueSky (BS) data

Table 1 summarises the experimental information including the number of epochs in each segment, the true position, and statistics on the number, C/N_0 and elevation of the observed satellites. The ID shown in the first column of the table consists of the test site and the orientation relative to the street. For example, T1_N represents that the data was collected on the north side of the street at test site T1 marked in Figure 7.

Table 1: Experimental information

ID	No. of epochs	True position coordinates, m (Easting, Northing)	Average No. of signals	Mean & SD* C/N_0, dB-Hz	Mean & SD* elevation, degrees	No. of satellites affected by map discrepancies
T1_N	120	(529455.33, 182345.04)	19.0	35.9, 9.0	38.3, 22.6	2
T1_S	120	(529458.74, 182339.39)	17.9	36.2, 10.0	39.3, 23.8	1
T2_N	119	(529523.09, 182208.10)	17.0	35.6, 10.8	41.7, 22.5	2
T2_S	120	(529529.08, 182199.13)	16.8	36.3, 10.5	41.4, 22.5	2
T3_W	119	(529383.08, 182290.97)	20.0	32.1, 8.2	38.5, 21.0	1
T3_E	120	(529389.38, 182295.83)	18.4	34.6, 10.6	40.6, 20.4	2
T4_W	120	(529410.39, 182250.62)	21.0	33.5, 8.0	37.7, 20.8	3
T4_E	119	(529416.02, 182254.40)	19.2	35.7, 8.4	40.1, 21.3	3

* SD stands for standard deviation.

Figure 11 in Appendix A illustrates the sky plots generated from, respectively, the OS and BS maps at the true location of each test site, where the coloured dots represent observed satellites and the blue lines delineate the minimum elevation angles of the LOS satellite (i.e. the building boundary), with satellites above the boundary predicted to be LOS (indicated in green) and those below the boundary predicted to be NLOS (indicated in red). The sky plots confirm that some satellite visibility can be incorrectly predicted due to the use of inaccurate 3D mapping data.

To validate the effectiveness of the proposed outlier detection methods for 3DMA GNSS positioning, the following algorithms were implemented, tested and compared:

- Conv: Single-epoch conventional GNSS with terrain height aiding
- S1: Single-epoch 3DMA GNSS without outlier detection
- S2: Single-epoch 3DMA GNSS with the sequential testing method described in Section III.2
- S3: Single-epoch 3DMA GNSS with the subset comparison method described in Section III.3

- M1: Multi-epoch 3DMA GNSS particle filter without outlier detection
- M2: Multi-epoch 3DMA GNSS particle filter with the sequential testing method described in Section III.2
- M3: Multi-epoch 3DMA GNSS particle filter with the subset comparison method described in Section III.2

The single-epoch conventional GNSS positioning solution was computed for comparison without the use of building model. On the high accuracy map provided by BS, the single-epoch 3DMA GNSS positioning algorithm without outlier detection was executed to determine the performance of 3DMA GNSS positioning in the absence of obvious mapping errors.

IV.2. Selection of Parameters

The 3DMA GNSS algorithms contain several empirical parameters that need to be determined in advance. Therefore, another dataset collected with the same equipment and configuration at different locations in the City of London on different dates was used to tune the parameters in the 3DMA GNSS algorithm, ensuring that the tuning and testing data were completely independent of each other.

The two thresholds mentioned in Sections III.2 and III.3 for outlier determination were determined after a range of different values were tried. Figure 9 shows the horizontal RMS errors for the single epoch 3DMA GNSS algorithm using OS maps with, respectively, sequential testing method and subset comparison method at different thresholds. Therefore, 3 and 2.5 are chosen as the thresholds for outlier determination for the sequential testing and subset comparison methods, respectively.

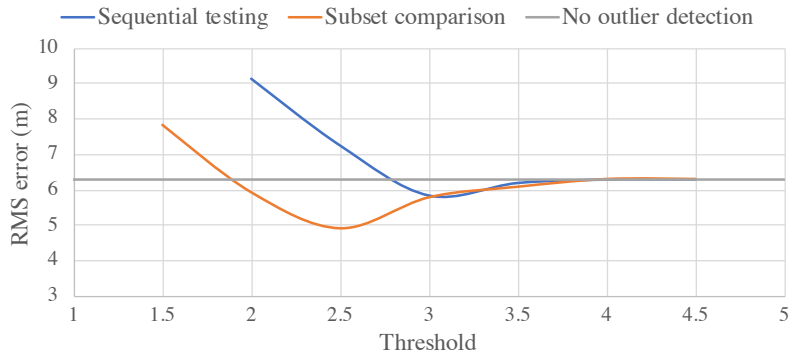

Figure 9: Selection of thresholds for outlier determination (single-epoch positioning, OS map)

IV.3. Experimental Results

Figure 10 shows the root mean square (RMS) horizontal position errors obtained from the tests on the dataset collected from the four experimental sites in London. As all methods include a terrain height aiding technique, only errors in the horizontal radial direction were assessed. The grey bar in Figure 10 represents the conventional GNSS positioning results, while the other coloured bars represent, respectively, the positioning results of the single- and multi-epoch 3DMA GNSS algorithm without and with different outlier detection methods on maps with different LoDs. Detailed results are presented in Figures 12 to 19 and Tables 2 to 4 in Appendix A.

The results show a significant improvement in accuracy of all 3DMA GNSS positioning algorithms involved in the experiment compared to conventional GNSS positioning. Compared to the 3DMA GNSS positioning using OS LoD1 maps, the one using BS LoD2 maps shows a clear lead in accuracy in all tests except for the test site T3_E, indicating that the accuracy of the maps does affect the accuracy of 3DMA GNSS. As shown in Figure 10, in single-epoch positioning without outlier detection, for example, the overall RMS error of the 3DMA GNSS solution using BS maps is nearly 30% smaller than that using the less accurate OS maps, especially at T2_S where this difference even reaches about 75%.

However, the mapping quality is not the only factor that largely influences the performance of 3DMA GNSS positioning. It can be clearly seen from Figures 12 to 19 that there are some significant fluctuations in the single-epoch 3DMA GNSS results, regardless of the accuracy of the maps used, which could be due to transient effects on the GNSS signals caused by passing vehicles. The positioning performance at test site T3 is significantly worse than the other test locations, and the difference in performance using OS and BS maps is not significant, suggesting that the main factor constraining 3DMA GNSS performance at T3 may not be mapping errors.

The experimental results also show that outlier detection has a greater impact on the results using OS maps than that using BS maps. In the case of single-epoch positioning with OS maps, according to the RMS position errors shown in Figure 10,

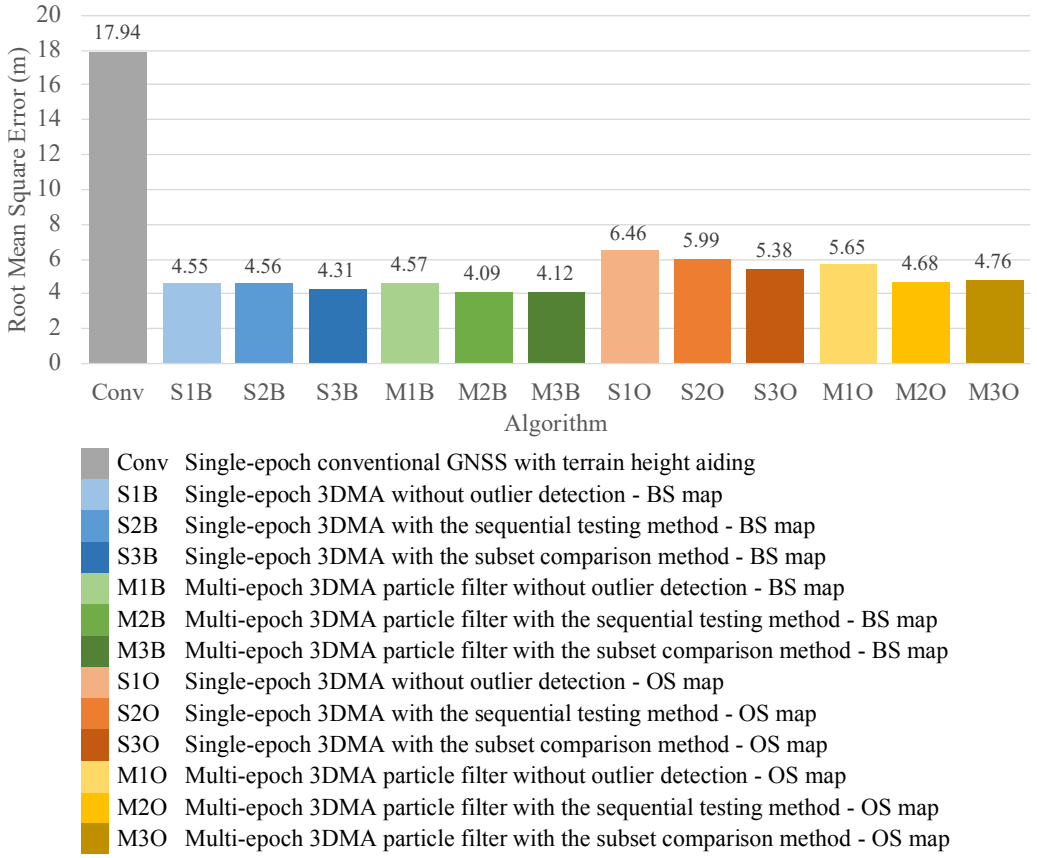

Figure 10: Horizontal radial position root mean square (RMS) error of the 3DMA GNSS algorithms with BS and OS maps

the 3DMA GNSS algorithms with subset comparison method applied achieved an overall performance improvement of around 15% compared to the one without. A closer investigation of the single-epoch GNSS results for each of the test sites presented in Table 2 in Appendix A reveals that subset comparison method is most effective in Sites T1_S and T4_W, achieving an improvement of more than 20% in RMS error. However, in the remaining sites, the algorithms with outlier detection do not show a major numerical improvement compared to the one without. In addition, compared to the case without outlier detection, the single-epoch results with outlier detection show a 20% reduction in the maximum error at the 90% confidence level, while the maximum error at the 50% confidence level rises by only 7%, indicating that outlier detection makes a significant contribution to the reliability of the 3DMA GNSS positioning. In the case of using BS maps, the improvement in RMS error due to outlier detection is not significant.

The main reason behind the outlier detection not performing as expected at some test sites may be the false alarms and missed detections. Both the SM and LBR algorithms are based on statistics and already include a certain amount of fault tolerance. Therefore, outlier detection for them is difficult. When some of the critical faulty measurements, such as those incorrectly selected as reference satellites in LBR, are detected and excluded, the solution is improved substantially. However, instead of improving performance, the exclusion of some less critical faulty measurements may increase uncertainty and weaken the effectiveness of outlier detection. Another possible reason for weakening the effectiveness of outlier detection is the increased uncertainty due to the exclusion of measurements. With the exclusion of some potential outliers, the solution for one of SM and LBR may be improved, while the other may suffer an increase in uncertainty due to the reduced number of measurements, thus diminishing the effectiveness of outlier detection. A possible mitigation option is to correct the faulty measurements to allow them to contribute to the positioning again, rather than eliminating them outright.

The introduction of filtering algorithms enhances the performance of 3DMA GNSS positioning. As illustrated in Figure 10, the multi-epoch 3DMA GNSS shows a reduction in RMS error of about 12% when using OS maps, while only a slight difference is shown when using BS maps. The filtering algorithm adjusts the 3DMA GNSS search area according to the previous position solution, reducing the occurrence of ambiguity problems and alleviating the problem of large sudden shifts in the position solution compared to the previous epoch caused by temporary environmental changes. It can be observed in Figures 12 to 19

that the error variation curves are smoother for the multi-epoch 3DMA GNSS compared to the single-epoch, demonstrating the filter's role in improving reliability.

As expected, the multi-epoch 3DMA GNSS with outlier detection performed best in the tests compared to the other algorithms. In the case of using OS maps, its performance rivals that of using BS LoD2 maps. This improvement is attributed to the combination of filtering and outlier detection. The mixture of mapping errors and temporary environmental changes makes it difficult for 3DMA outlier detection algorithms to handle them properly at the same time. The filtering creates a better search area for 3DMA GNSS based on the solution from the previous epoch. Outlier detection, in return, brings a further improvement of about 16% compared to multi-epoch 3DMA GNSS without outlier detection.

The performance of the sequential testing method and the subset comparison method is similar in multi-epoch positioning, while the subset comparison method is superior in single-epoch case. This may be because when the sequential testing method incorrectly excludes some measurements, the remaining consistently misleads the outlier algorithm to further exclude good measurements, whereas the subset comparison method focuses only on measurements in the consensus set and is less affected by noise. In terms of computational efficiency, the sequential method is more efficient than subset comparison method.

V. CONCLUSIONS

The results of the experiments conducted in London confirm that 3D mapping errors can have a noticeable negative impact on the performance of 3DMA GNSS positioning. At all test sites except site T3, the horizontal RMS position error of the 3DMA GNSS algorithm using the high accuracy LoD2 map provided by BS is between 2 and 3 metres, which is significantly lower than that using the OS map with significant mapping errors.

Two outlier detection methods were introduced into the 3DMA GNSS algorithm. The sequential detection method uses test statistics in the measurement domain to directly exclude the suspected faulty measurements, while the subset comparison method uses test statistics in the position domain to evaluate the consensus sets found by the test statistics in the measurement domain and leaves the most consistent ones. The performance of the sequential test and the subset comparison methods are similar, probably because they use the same test statistics. For single-epoch 3DMA GNSS, after applying outlier detection, the 3DMA GNSS algorithm reduced the RMS horizontal position error by approximately 15% compared to the original, but still worse than 3DMA GNSS with BS maps. The proposed outlier detection methods are most effective at test sites T1_S and T4_W, and result in an improvement in RMS position error of more than 30%. However, at the other test sites, the outlier detection algorithms deliver a limited improvement and do not perform as good as expected, suggesting that more time is needed to improve them.

The interplay of mapping data errors and temporary environmental changes makes it difficult for outlier detection to handle multiple outlying measurements properly at the same time. The introduction of filtering provides 3DMA GNSS with a priori information to define the search area, allowing the latter to find outlying measurements more easily. The final results also show that the 3DMA filtering with outlier detection performs the best of all the algorithms in this test, and its performance with OS LoD1 maps rivals that of BS LoD2 maps.

VI. FUTURE WORK

The current version of the outlier detection algorithms for 3DMA GNSS positioning is still in its early stages and has much room for improvement. Areas worth exploring further include:

- Correction of outlying measurements to allow them to re-contribute to positioning.

  Directly removing outliers may not only increase the uncertainty in the shadow matching solution, but may also degrade the satellite geometry in likelihood-based ranging. Thus, the outliers may be able to be corrected by correcting the corresponding satellite visibility predictions so that they can re-contribute to the positioning and improve the quality of the solution.

- Flagging of mapping data errors.

  Inspired by the idea of simultaneous localization and mapping (SLAM) and the paper [39], incorrect building information can be flagged (or corrected if possible) to benefit subsequent measurements.

ACKNOWLEDGEMENTS

Qiming Zhong is funded by the China Scholarship Council and a UCL Engineering Faculty Scholarship. The authors are also grateful to James Quick for providing the dataset used for testing.

APPENDIX A DETAILED EXPERIMENTAL RESULTS

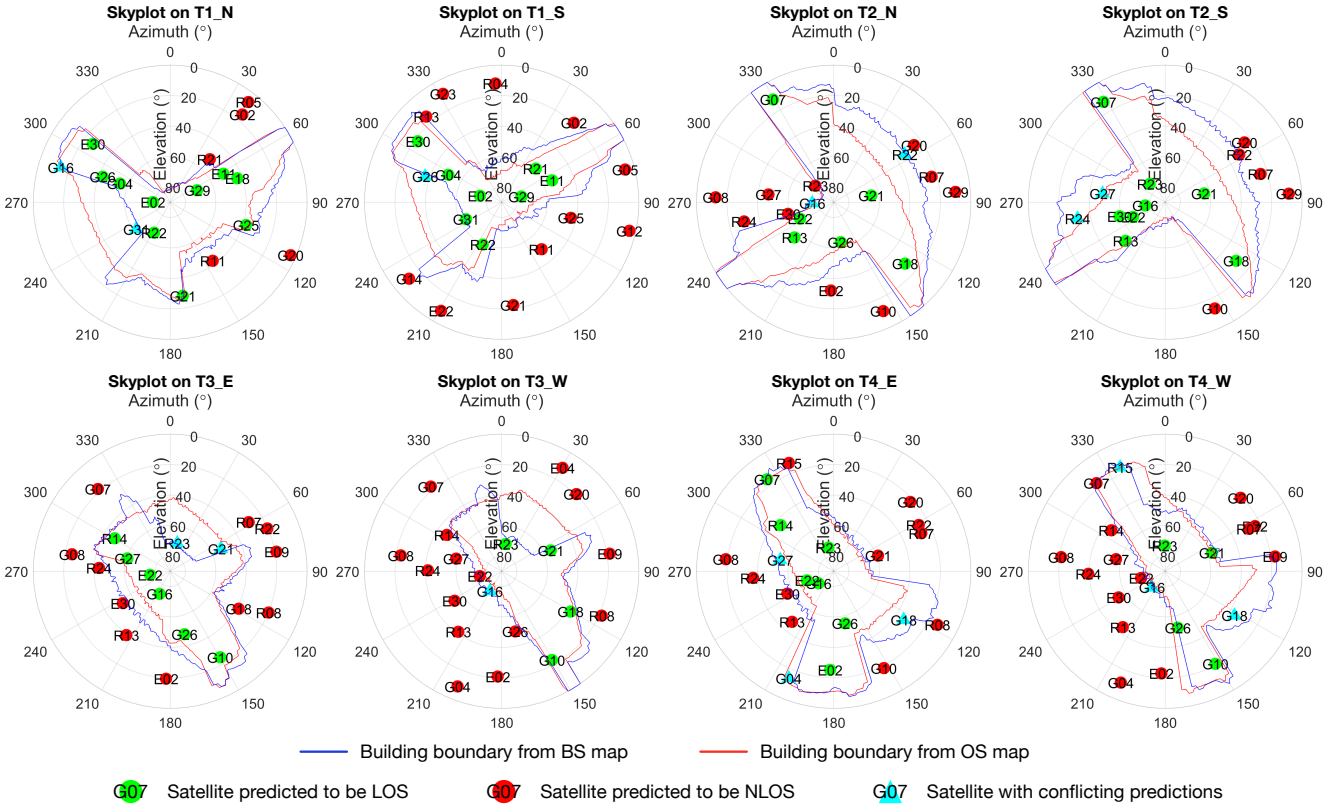

Figure 11: Sky plots generated from Ordnance Survey (OS) and BlueSky (BS) maps at Epoch 1 at the true location of each test site

List of abbreviations for the labels in Figures 12 to 19 and Tables 2 to 4

Conv	Single-epoch conventional GNSS with terrain height aiding
S1B	Single-epoch 3DMA without outlier detection - BS map
S2B	Single-epoch 3DMA with the sequential testing method - BS map
S3B	Single-epoch 3DMA with the subset comparison method - BS map
M1B	Multi-epoch 3DMA particle filter without outlier detection - BS map
M2B	Multi-epoch 3DMA particle filter with the sequential testing method - BS map
M3B	Multi-epoch 3DMA particle filter with the subset comparison method - BS map
S1O	Single-epoch 3DMA without outlier detection - OS map
S2O	Single-epoch 3DMA with the sequential testing method - OS map
S3O	Single-epoch 3DMA with the subset comparison method - OS map
M1O	Multi-epoch 3DMA particle filter without outlier detection - OS map
M2O	Multi-epoch 3DMA particle filter with the sequential testing method - OS map
M3O	Multi-epoch 3DMA particle filter with the subset comparison method - OS map

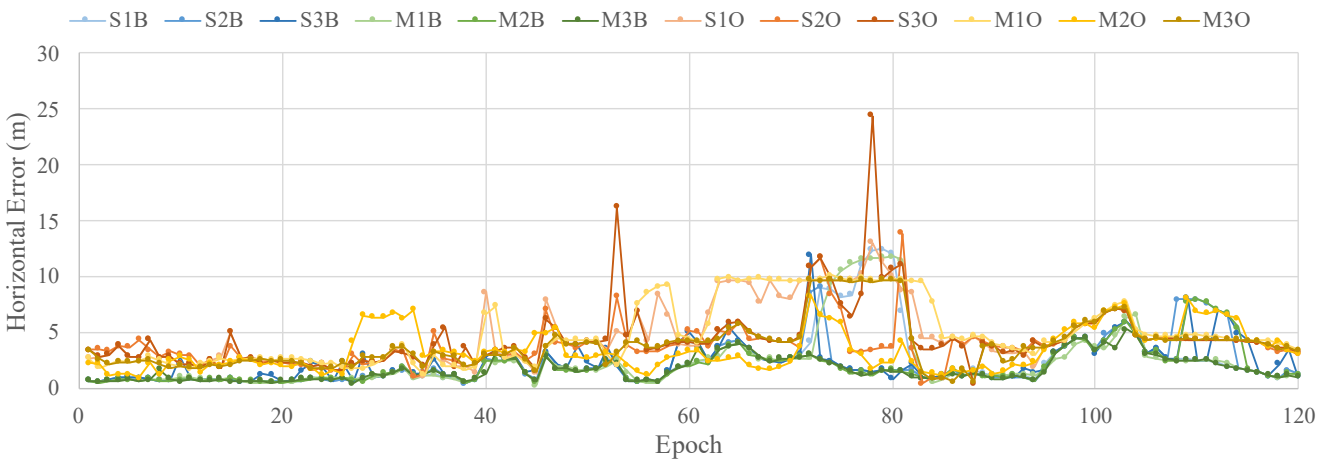

Figure 12: Horizontal position errors for the solutions of the 3DMA GNSS algorithms on test site T1_N

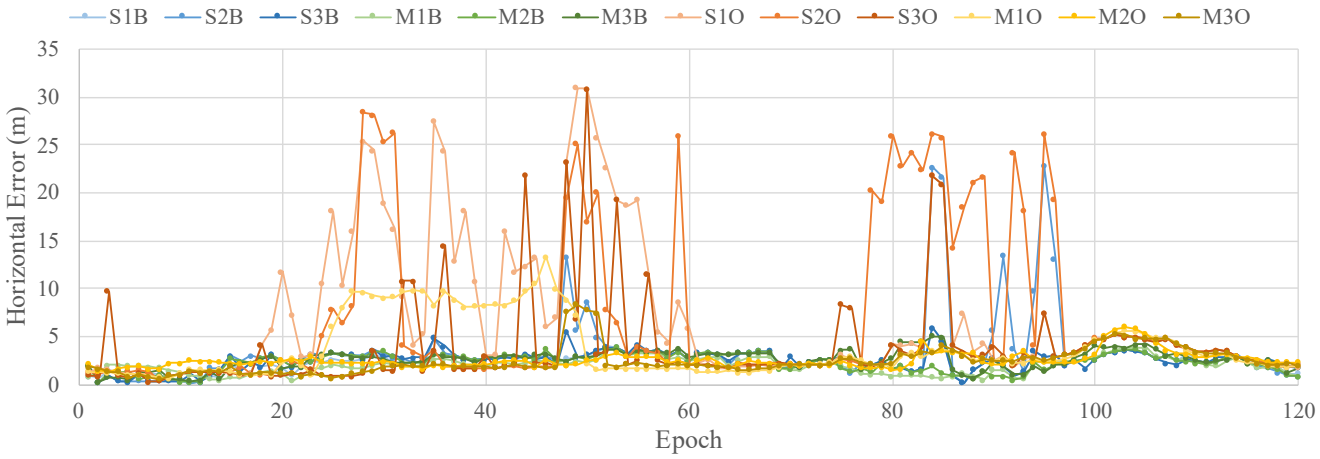

Figure 13: Horizontal position errors for the solutions of the 3DMA GNSS algorithms on test site T1_S

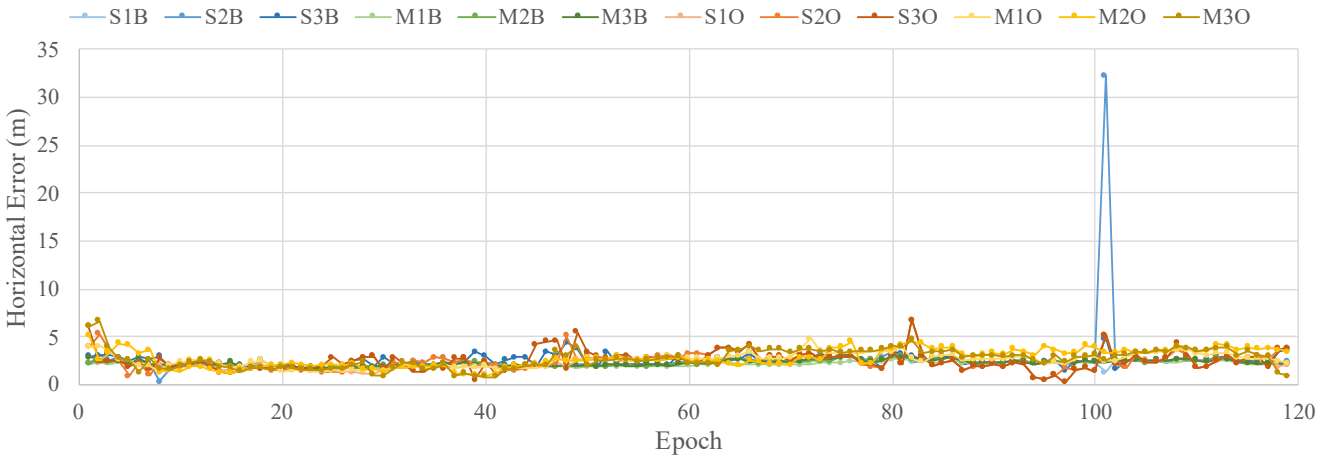

Figure 14: Horizontal position errors for the solutions of the 3DMA GNSS algorithms on test site T2_N

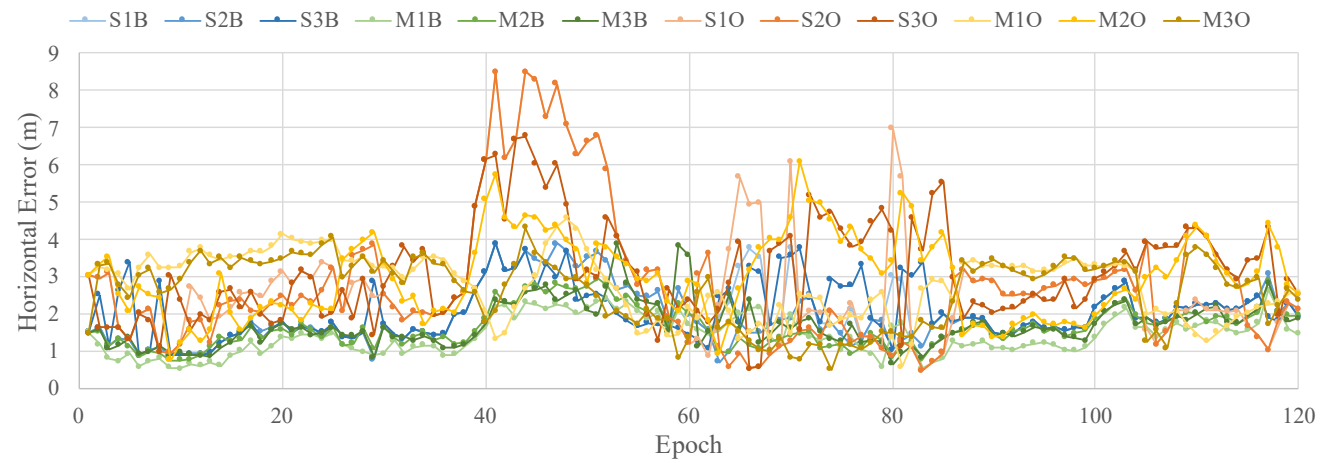

Figure 15: Horizontal position errors for the solutions of the 3DMA GNSS algorithms on test site T2_S

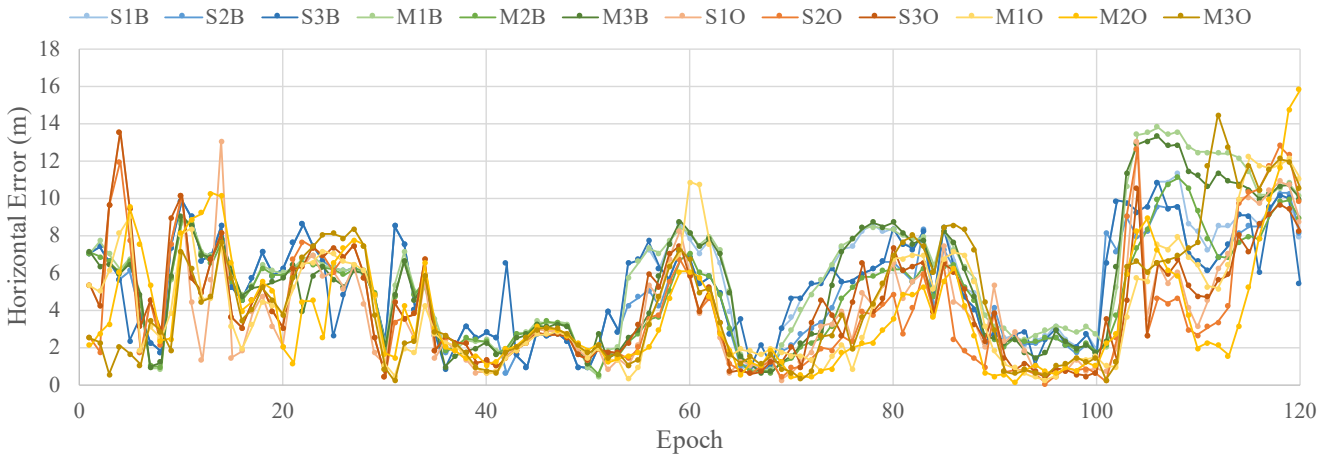

Figure 16: Horizontal position errors for the solutions of the 3DMA GNSS algorithms on test site T3_E

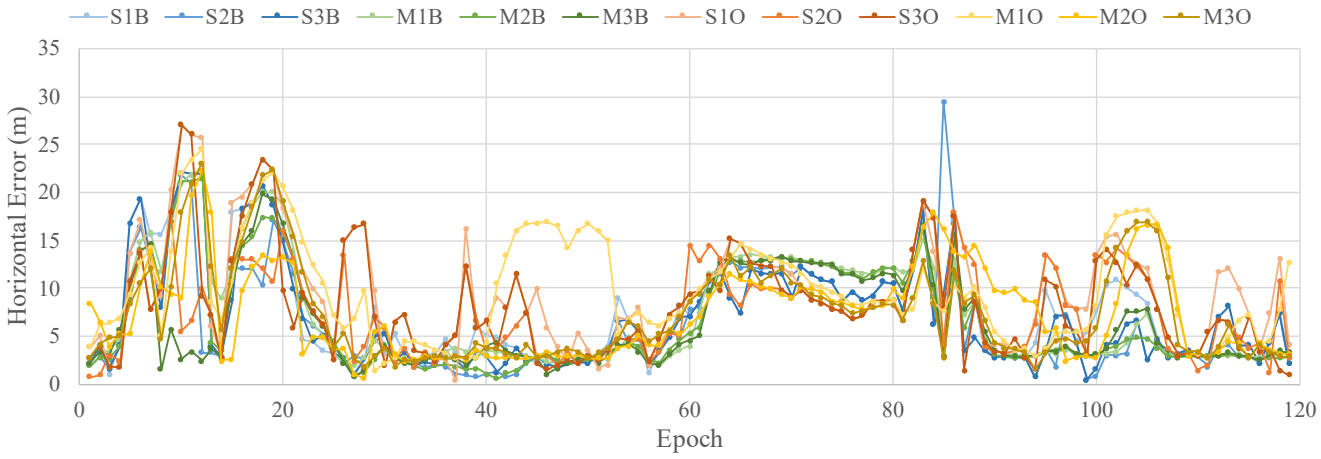

Figure 17: Horizontal position errors for the solutions of the 3DMA GNSS algorithms on test site T3_W

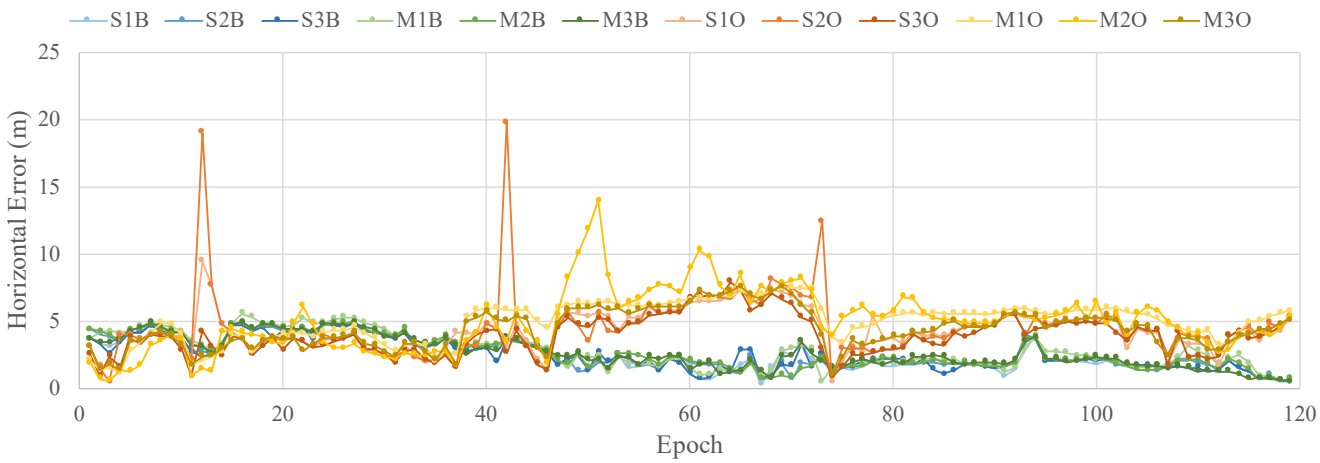

Figure 18: Horizontal position errors for the solutions of the 3DMA GNSS algorithms on test site T4_E

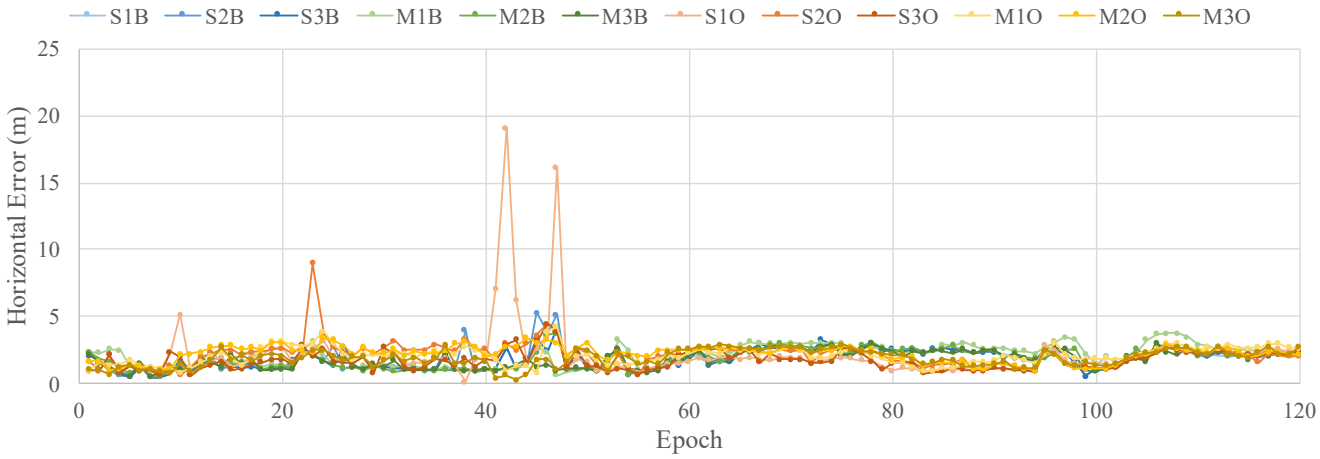

Figure 19: Horizontal position errors for the solutions of the 3DMA GNSS algorithms on test site T4_W

Table 2: Horizontal radial position RMS errors (in metres)

Algorithm	Test site							
	T1_N	T1_S	T2_N	T2_S	T3_W	T3_E	T4_W	T4_E
Conv	15.43	17.20	5.76	8.75	29.82	19.60	18.16	18.18
S1B	3.52	2.55	2.37	2.19	9.26	6.29	1.96	2.79
S2B	2.97	5.00	3.79	2.06	8.34	5.69	2.07	2.82
S3B	2.92	2.69	2.62	2.20	8.66	5.92	2.01	2.78
M1B	3.60	2.13	2.15	1.51	9.01	6.88	2.28	3.08
M2B	2.60	2.45	2.32	1.72	8.41	5.42	2.00	2.92
M3B	2.08	2.73	2.34	1.81	7.83	6.47	1.91	2.91
S1O	5.45	10.18	2.56	3.47	11.22	5.13	3.06	4.56
S2O	4.39	10.83	2.66	3.30	8.68	4.96	2.36	5.21
S3O	5.36	6.38	2.72	3.38	9.85	5.11	1.88	4.16
M1O	5.63	4.76	2.70	2.90	11.26	5.26	2.22	5.17
M2O	3.91	2.66	2.95	3.19	8.70	4.85	2.32	5.47
M3O	4.50	2.81	2.93	2.77	9.04	5.50	2.02	4.62

Table 3: Maximum horizontal radial position error (in metres) at 90% confidence level

Algorithm	Test site							
	T1_N	T1_S	T2_N	T2_S	T3_W	T3_E	T4_W	T4_E
Conv	23.36	21.47	11.08	13.27	37.73	33.40	21.87	26.01
S1B	5.11	3.45	2.86	3.35	17.84	9.12	2.69	4.35
S2B	4.92	4.83	2.88	3.18	12.74	8.50	2.70	4.37
S3B	4.46	3.54	3.38	3.25	17.58	9.12	2.69	4.34
M1B	4.71	2.92	2.55	2.18	15.06	11.41	3.10	4.83
M2B	4.35	3.36	2.69	2.49	14.36	8.31	2.77	4.47
M3B	3.55	3.75	2.75	2.51	13.16	10.72	2.58	4.55
S1O	9.67	19.30	3.45	6.19	18.24	9.46	2.64	6.46
S2O	5.92	24.21	3.77	6.15	13.84	9.00	2.74	6.85
S3O	6.96	8.37	3.84	4.90	16.74	8.10	2.63	5.81
M1O	9.75	9.13	3.48	3.78	17.93	8.17	3.00	6.78
M2O	6.60	3.32	4.02	4.56	14.27	8.10	2.94	8.02
M3O	7.19	4.57	3.89	3.59	15.91	8.47	2.74	6.42

Table 4: Maximum horizontal radial position error (in metres) at 50% confidence level

Algorithm	Test site							
	T1_N	T1_S	T2_N	T2_S	T3_W	T3_E	T4_W	T4_E
Conv	13.83	17.03	3.08	7.61	29.98	12.89	17.89	17.74
S1B	1.60	2.43	2.34	1.85	6.18	6.23	1.97	2.15
S2B	1.57	2.64	2.34	1.76	4.09	5.50	1.97	2.16
S3B	1.76	2.63	2.50	1.88	4.82	5.67	2.01	2.19
M1B	1.44	2.00	2.12	1.39	3.78	6.11	2.31	2.49
M2B	1.46	2.40	2.31	1.54	3.93	5.03	1.97	2.24
M3B	1.43	2.71	2.28	1.59	3.66	5.64	1.89	2.36
S1O	4.10	3.67	2.29	2.51	8.66	3.56	1.76	4.18
S2O	3.70	2.62	2.46	2.42	6.74	2.93	2.26	4.10
S3O	4.03	2.18	2.39	2.95	7.28	3.91	1.66	3.92
M1O	4.28	2.51	2.70	3.03	8.69	3.34	2.12	5.50
M2O	2.93	2.31	2.72	2.93	6.07	2.66	2.37	4.89
M3O	3.75	2.02	2.83	2.95	5.76	3.41	1.97	4.22

REFERENCES

[1] P. D. Groves, *Principles of GNSS, inertial, and multisensor integrated navigation systems*. Boston; London: Artech House, 2013.

[2] Y. Yuan, F. Shen, and X. Li, "GPS multipath and NLOS mitigation for relative positioning in urban environments," *Aerospace Science and Technology*, vol. 107, p. 106315, dec 2020.

[3] P. D. Groves, Z. Jiang, M. Rudi, and P. Strode, "A portfolio approach to NLOS and multipath mitigation in dense urban areas," *26th International Technical Meeting of the Satellite Division of the Institute of Navigation, ION GNSS 2013*, vol. 4, no. September, pp. 3231–3247, 2013.

[4] H. F. Ng, G. Zhang, and L. T. Hsu, "Robust GNSS Shadow Matching for Smartphones in Urban Canyons," *IEEE Sensors Journal*, vol. 21, no. 16, pp. 18 307–18 317, 2021. [Online]. Available: https://ieeexplore.ieee.org/abstract/document/9440901/

[5] L. T. Hsu, S. S. Jan, P. D. Groves, and N. Kubo, "Multipath mitigation and NLOS detection using vector tracking in urban environments," *GPS Solutions*, vol. 19, no. 2, pp. 249–262, jun 2015. [Online]. Available: https://link.springer.com/article/10.1007/s10291-014-0384-6

[6] P. D. Groves, Q. Zhong, R. Faragher, and P. Esteves, "Combining inertially-aided extended coherent integration (Super-correlation) with 3D-mapping-aided GNSS," in *Proceedings of the 33rd International Technical Meeting of the Satellite Division of the Institute of Navigation, ION GNSS+ 2020*. Institute of Navigation (ION), sep 2020, pp. 2327–2346.

[7] L. T. Hsu, Y. Gu, and S. Kamijo, "3D building model-based pedestrian positioning method using GPS/GLONASS/QZSS and its reliability calculation," *GPS Solutions*, vol. 20, no. 3, pp. 413–428, 2016.

[8] T. Suzuki and N. Kubo, "Correcting GNSS multipath errors using a 3D surface model and particle filter," *26th International Technical Meeting of the Satellite Division of the Institute of Navigation, ION GNSS 2013*, vol. 2, pp. 1583–1595, 2013.

[9] N. I. Ziedan, "Enhancing GNSS mobile positioning in urban environments through utilization of multipath prediction and consistency analysis," *Proceedings of the 32nd International Technical Meeting of the Satellite Division of the Institute of Navigation, ION GNSS+ 2019*, pp. 3469–3483, 2019.

[10] F. Biljecki, G. B. Heuvelink, H. Ledoux, and J. Stoter, "The effect of acquisition error and level of detail on the accuracy of spatial analyses," *Cartography and Geographic Information Science*, vol. 45, no. 2, pp. 156–176, mar 2018. [Online]. Available: https://www.tandfonline.com/doi/abs/10.1080/15230406.2017.1279986

[11] S. Ji, W. Chen, X. Ding, Y. Chen, C. Zhao, and C. Hu, "Potential benefits of GPS/GLONASS/GALILEO integration in an urban canyon - Hong Kong," *Journal of Navigation*, vol. 63, no. 4, pp. 681–693, oct 2010.

[12] K. Nur, S. Feng, C. Ling, and W. Ochieng, "Integration of GPS with a WiFi high accuracy ranging functionality," *Geo-Spatial Information Science*, vol. 16, no. 3, pp. 155–168, sep 2013.

[13] T. H. Kolbe, T. Kutzner, C. S. Smyth, C. Nagel, C. Roensdorf, and C. Heazel, *OGC City Geography Markup Language (CityGML) Part 1: Conceptual Model Standard*. Open Geospatial Consortium, 2021.

[14] M.-O. Löwner, G. Gröger, J. Benner, F. Biljecki, and C. Nagel, "Proposal for a new LOD and multi-representation concept for CityGML," *ISPRS Ann Photogramm Remote Sens Spatial Inf Sci*, vol. 4, pp. 3–12, 2016.

[15] P. D. Groves, "Shadow matching: A new GNSS positioning technique for urban canyons," *Journal of Navigation*, vol. 64, no. 3, pp. 417–430, jul 2011.

[16] C. Tiberius and E. Verbree, "GNSS positioning accuracy and availability within Location Based Services: The advantages of combined GPS-Galileo positioning," in *NaviTec*, 2004.

[17] S. S. Saab and Z. M. Kassas, "Power matching approach for GPS coverage extension," *IEEE Transactions on Intelligent Transportation Systems*, vol. 7, no. 2, pp. 156–166, 2006.

[18] B. Ben-Moshe, E. Elkin, H. Levi, and A. Weissman, "Improving accuracy of GNSS devices in urban canyons," *Proceedings of the 23rd Annual Canadian Conference on Computational Geometry, CCCG 2011*, 2011.

[19] L. Wang, P. D. Groves, and M. K. Ziebart, "GNSS Shadow Matching Using A 3D Model of London," in *European Navigation Conference*, dec 2011.

[20] L. Wang, P. D. Groves, and M. K. Ziebart, "Smartphone shadow matching for better cross-street GNSS positioning in urban environments," *Journal of Navigation*, vol. 68, no. 3, pp. 411–433, 2015.

[21] L. Wang, P. D. Groves, and M. K. Ziebart, "Urban positioning on a smartphone: Real-time shadow matching using GNSS and 3D City Models," *26th International Technical Meeting of the Satellite Division of the Institute of Navigation, ION GNSS 2013*, vol. 2, pp. 1606–1619, sep 2013.

[22] L. Wang, "Investigation of Shadow Matching for GNSS Positioning in Urban Canyons," Ph.D. dissertation, University College London, 2015.

[23] J. T. Isaacs, A. T. Irish, F. Quitin, U. Madhow, and J. P. Hespanha, "Bayesian localization and mapping using GNSS SNR measurements," in *Record - IEEE PLANS, Position Location and Navigation Symposium*, 2014, pp. 445–451.

[24] G. Zhang, W. Wen, B. Xu, and L. T. Hsu, "Extending Shadow Matching to Tightly-Coupled GNSS/INS Integration System," *IEEE Transactions on Vehicular Technology*, vol. 69, no. 5, pp. 4979–4991, may 2020.

[25] R. Yozevitch and B. ben Moshe, "A Robust Shadow Matching Algorithm for GNSS Positioning," *Navigation, Journal of the Institute of Navigation*, vol. 62, no. 2, pp. 95–109, sep 2015.

[26] M. Obst, S. Bauer, and G. Wanielik, "Urban multipath detection and mitigation with dynamic 3D maps for reliable land vehicle localization," in *Record - IEEE PLANS, Position Location and Navigation Symposium*, 2012, pp. 685–691.

[27] S. Peyraud, D. Bètaille, S. Renault, M. Ortiz, F. Mougel, D. Meizel, and F. Peyret, "About non-line-of-sight satellite detection and exclusion in a 3D map-aided localization algorithm," *Sensors (Switzerland)*, vol. 13, no. 1, pp. 829–847, 2013.

[28] H. F. Ng and L. T. Hsu, "3D Mapping Database Aided GNSS RTK and Its Assessments in Urban Canyons," *IEEE Transactions on Aerospace and Electronic Systems*, 2021.

[29] L. T. Hsu, Y. Gu, and S. Kamijo, "NLOS correction/exclusion for GNSS measurement using RAIM and city building models," *Sensors (Switzerland)*, vol. 15, no. 7, pp. 17 329–17 349, jul 2015.

[30] Y. Gu and S. Kamijo, "GNSS positioning in deep urban city with 3D map and double reflection," in *2017 European Navigation Conference, ENC 2017*. Institute of Electrical and Electronics Engineers Inc., jun 2017, pp. 84–90.

[31] G. Zhang, H.-F. Ng, W. Wen, and L.-T. Hsu, "3D Mapping Database Aided GNSS Based Collaborative Positioning Using Factor Graph Optimization," *IEEE Transactions on Intelligent Transportation Systems*, pp. 1–13, apr 2020.

[32] Q. Zhong and P. D. Groves, "Multi-epoch 3d-mapping-aided positioning using bayesian filtering techniques," *NAVIGATION: Journal of the Institute of Navigation*, vol. 69, no. 2, 2022. [Online]. Available: https://navi.ion.org/content/69/2/navi.515

[33] V. Barnett and T. Lewis, "Outliers in statistical data john wiley and sons," *New York*, 1994.

[34] F. E. Grubbs, "Procedures for detecting outlying observations in samples," *Technometrics*, vol. 11, no. 1, pp. 1–21, 1969.

[35] F. Biljecki, "Level of detail in 3D city models," Ph.D. dissertation, Delft University of Technology, 2017. [Online]. Available: https://repository.tudelft.nl/islandora/object/uuid%3A6fe1dea8-53b3-4734-9e0c-ff01ed393d79

[36] Ordnance Survey, "OS MasterMap Topography Layer support." [Online]. Available: https://www.ordnancesurvey.co.uk/business-government/tools-support/mastermap-topography-support

[37] Ordnance Survey, "OS MasterMap® Topography Layer-Building Height Attribute Product Guide," 2020. [Online]. Available: www.os.uk

[38] P. D. Groves and Z. Jiang, "Height aiding, C/N0 weighting and consistency checking for GNSS NLOS and multipath mitigation in urban areas," *Journal of Navigation*, vol. 66, no. 5, pp. 653–669, sep 2013.

[39] T. Lines and A. Basiri, "3D map creation using crowdsourced GNSS data," *Computers, Environment and Urban Systems*, vol. 89, p. 101671, sep 2021.